Applications in Energy and Combustion Science 21 (2025) 100321

Contents lists available at ScienceDirect

Applications in Energy and Combustion Science

journal homepage: www.elsevier.com/locate/jaecs

Observing simultaneous low temperature heat release and deflagration in a spark ignition engine using formaldehyde planar laser induced fluorescence

Samuel P. White, Christopher Willman, Felix C.P. Leach *

Department of Engineering Science, Parks Road, Oxford, OX1 3PJ, UK

ARTICLE INFO

Keywords:
PLIF
Formaldehyde
LTHR
PRF

ABSTRACT

Low temperature heat release (LTHR) and its underlying chemistry is of particular interest for its potential to mitigate knock in spark ignition (SI) engines and enable advanced combustion strategies that rely on end gas autoignition. It has been proposed that, in SI engines, LTHR can occur volumetrically in the end gas, after ignition, whilst deflagration occurs elsewhere in the cylinder, however, current pressure-based heat release metering techniques are unable to distinguish such LTHR from high temperature heat release (HTHR) due to the overlapping pressure rise characteristics. Planar laser-induced fluorescence (PLIF) of formaldehyde, a known product of LTHR which is consumed during HTHR, offers an opportunity to detect end gas LTHR simultaneously with deflagration but is challenging to implement, as end gas is often located closer to cylinder walls and away from typical optically accessible locations. An optically accessible SI engine was used to show formaldehyde PLIF signal intensity under motored conditions is well correlated to cumulative LTHR intensity, using a recent method to isolate LTHR in SI engine conditions. An alternative ignition method using four side-mounted spark plugs was implemented to generate end gas close to the cylinder axis. This enabled measurement of LTHR within the end gas during the deflagration process of a SI engine, demonstrating the utility of formaldehyde PLIF to optically measure LTHR under conditions where pressure-based diagnostics cannot isolate the contribution of LTHR.

1. Introduction

The overall CO_2 emissions of light-duty vehicles can be reduced by increasing internal combustion engine efficiency and using fuels and fuel sources that are less carbon-intensive [1]. Knocking, unwanted and uncontrolled autoignition of end gas (the portion of the fuel-air mixture ahead of the flame), is one of the main factors limiting engine operation and efficiency [2]. The high-frequency, high-pressure oscillations associated with the occurrence of knock can cause significant damage to many different engine components, hence it must be avoided. Knocking can occur when the pressure and temperature of the end gas spend enough time above a certain threshold, leading to spontaneous autoignition [3]. The specific delay time, pressure and temperature at which autoignition occurs depends on the composition of the mixture and therefore the choice of fuel and any intermediate reactions that have occurred in the meantime.

Leppard showed that, for alkane fuels, the autoignition chemistry is dominated by negative temperature coefficient (NTC) behaviour [4]. This is where, at certain conditions, the reaction rate is inversely proportional to temperature. This leads to two distinct stages of the ignition process. Low temperature heat release (LTHR) is followed by the NTC region (characterised by a pause in heat release) and subsequently, high temperature heat release (HTHR), where knocking can occur. Since then, LTHR has been observed in homogeneous charge compression ignition (HCCI) engines [5–7].

The low temperature reaction pathways that cause LTHR in the two primary reference fuels (PRFs), iso-octane and n-heptane, were examined in depth by Curran in comprehensive modelling studies [8, 9]. At low temperatures the PRFs first undergo hydrogen abstraction by OH, then two additions of O_2 and isomerisation reactions to form carbonylhydroperoxide species, which subsequently undergo low temperature chain branching, producing OH radicals. Alongside this, beta-decomposition of the various intermediate species leads to the formation of significant amounts of formaldehyde.

More recently, LTHR has been shown in SI engines, [10–12] where it is seen before the spark and hence termed pre-spark heat release (PSHR). Szybist and Splitter observed that PSHR was more likely to be seen in fuels with low octane sensitivity and at high load conditions with elevated inlet temperatures. Furthermore, Splitter et al. used elevated intake temperatures to show PSHR is related to knocking

* Corresponding author.
E-mail address: felix.leach@eng.ox.ac.uk (F.C.P. Leach).

https://doi.org/10.1016/j.jaecs.2025.100321
Received 25 September 2024; Received in revised form 17 December 2024; Accepted 15 January 2025
Available online 22 January 2025

chemistry [13]. They found that when PSHR occurred, the knock-limited combustion phasing was insensitive to intake temperature, with higher intake temperatures not requiring retarded ignition timings as they otherwise would. The occurrence of LTHR (as PSHR) caused the end gas to move into a thermodynamic state with a long ignition delay, which inhibited knock.

In SI engines (and unlike in HCCI engines), HTHR combustion occurs as a pre-mixed flame deflagration process which need not necessarily be preceded by the low-temperature pathways that exhibit LTHR, however, if it is, the chemical and thermodynamic properties of the end gas will have changed—changing the autoignition properties, including knocking. Hence, if LTHR can be understood better — and ultimately controlled — it has the potential to increase engine efficiency by extending the knocking limit [13] or by enabling high-efficiency advanced combustion strategies that involve spark-triggered flame propagation causing auto-ignition without triggering engine knock [14–17]. These advanced combustion strategies rely on curating specific chemical conditions in the end gas [18].

Splitter et al. used ignition delay analysis in a PSHR study to show that it is possible that, for some conditions that do not exhibit PSHR, as deflagration occurs the end gas region will traverse the same region in pressure-temperature space as cases that do exhibit PSHR, suggesting that bulk gas LTHR reactions in the end gas is probable [13]. Since these reactions change the species composition ahead of the flame, understanding them could be critical for understanding knocking behaviour in SI engines. However, as these authors highlighted, conventional pressure-based heat release analysis techniques are unable to experimentally observe end gas LTHR as its contribution to pressure rise would be indistinguishable from that of the heat released from deflagration. The aim of this work is to use alternatives to pressure-based diagnostic techniques to determine whether LTHR can occur in end gas at the same time as deflagration (elsewhere in the cylinder), for conditions with no observable PSHR. Hence an alternative method of experimentally observing LTHR must be determined.

Through past experimentation and work developing chemical kinetic mechanisms for the primary reference fuels, the reaction indicators and products of the low temperature oxidation pathways are relatively well known [8]. Indicators include the OH and HO_2 radicals and significant products include CO, H_2O_2, and CH_2O. The latter two are particularly significant as they are present in much larger quantities as products of first stage autoignition compared to as HTHR products [10,19], so have the potential to be used as markers for LTHR. Spatially and temporally resolved measurement of formaldehyde would therefore enable in-cylinder detection of the progression of LTHR processes within the end gas.

Optical diagnostic techniques enable gas-phase measurements within challenging environments, where measurements with physical sensors are either impossible or impractical [20–23].

For two-dimensional measurements, Laser-Induced Fluorescence (LIF) is widely used for species detection, using a laser sheet to excite the target species to a higher energy state and imaging the fluorescence emitted as the species returns to the ground state [24]. Selective detection of species is often achieved by utilising features in either the absorption or emission spectra of the target species, which allows multiple species to be detected simultaneously, such as OH, CH and formaldehyde, in flame reaction zone studies [25].

In the case of formaldehyde, absorption features around 355 nm overlap with the conveniently-accessible 3rd harmonic output of an Nd:YAG laser. While more efficient excitation is possible, targeting alternative excitation lines (e.g. 353.07 nm with a tuneable dye laser), the higher output energy of a tripled Nd:YAG typically more than compensates for the lower excitation efficiency [26,27] and allows for a simpler experimental setup.

Excitation of in-cylinder end gas at 355 nm may excite a range of LTHR products whose fluorescence cannot be distinguished from formaldehyde using broad spectral filters [28]. Multi-band filters can provide more selective detection of formaldehyde emission [29]; however, if the intention is to detect LTHR products, exact identification of the other fluorescing species is not necessary, only that they are generated during LTHR and consumed during HTHR [27]. This permits the use of LIF primarily targeting formaldehyde to investigate the end gas of SI engines to infer spatial temperature variations [30] and to identify sites of autoignition [31].

Formaldehyde LIF has been used to investigate the first stage of the ignition process in HCCI engines [27,32,33]. For PRF blends of iso-octane and n-heptane which exhibit NTC behaviour, LTHR in HCCI engines typically occurs earlier than, and distinct from, HTHR [34], enabling the use of either optical or pressure-based measurement techniques similarly to PSHR in SI engines [35]. Graf et al. used LIF to measure formaldehyde concentration in “cool-flame” (LTHR) events in an SI engine with PRF50 under HCCI conditions [36]. Their work is similar to this work in some ways, but measures LTHR prior to ignition with a centrally mounted spark plug. LTHR in end-gas is unobserved in their work.

LTHR processes continuing during deflagration has been observed using formaldehyde LIF in a Rapid Compression Machine (RCM) under Spark Induced Compression Ignition (SICI) conditions [37], however a significant pressure rise due to LTHR was observed before the main HTHR pressure rise, putting these SICI conditions in a similar regime to partially developed PSHR, which may also be measured using pressure-based methods [35].

This work uses formaldehyde LIF to demonstrate that LTHR occurring simultaneously with deflagration in an SI engine may be measured optically under conditions in which pressure-based measurement techniques cannot distinguish between the pressure rises associated with LTHR and HTHR processes.

Recent work by White et al. [38–40] and Bajwa et al. [41] introduced a methodology to isolate LTHR in a spark ignition engine by maintaining LTHR- and PSHR-prone inlet conditions whilst avoiding HTHR by disabling the ignition system. This can be used to test techniques for detecting LTHR with optical methods that observe non-pressure-based markers by comparing them to standard LTHR markers observed using the isolated methodology.

In this study, we seek to expand the understanding of the occurrence of LTHR in SI engines through the use of a formaldehyde LIF-based optical diagnostic method. 2D PLIF images will be analysed alongside measured apparent heat release rate and high-speed flame imaging to detect LTHR both in isolation and in end gas while deflagration is occurring elsewhere in the cylinder. LIF signals and LTHR measurements will be analysed to determine the efficacy of LIF as a diagnostic tool for observing LTHR in SI engines. In a fired engine, the ignition system is modified to produce central, optically accessible end gas, and formaldehyde PLIF is used to examine said central end gas during deflagration. The results of this study highlight the ability of non-pressure-derived diagnostic techniques to detect LTHR and subsequently answer the question of whether or not bulk gas LTHR reactions occur in the end gas concurrently with deflagration in SI engines.

2. Methodology

2.1. Experimental facility

Optical and pressure-based measurements of LTHR were performed in a single cylinder, optically accessible direct injection SI engine during motored and fired operation with two non-fluorescing fuels: n-heptane and a mixture of 15% (v/v) n-heptane and 85% 2,2,4-trimethylpentane (iso-octane) — PRF85. The specifications of the optically accessible engine are given in Table 1 and details of the instrumentation are supplied in Table 2.

Optical access to the engine (for imaging) was provided through a 60 mm central piston window. Considering the nature of this work — to image LTHR in the unburnt end gas — the last portion of the cylinder

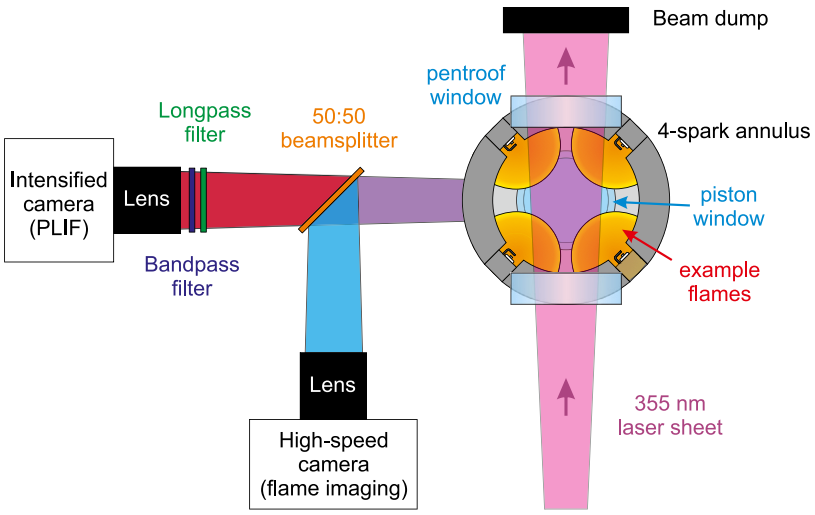

Fig. 1. Optical layout for formaldehyde PLIF and high-speed flame imaging. A 355 nm laser sheet passes through a pair of opposed pentroof windows. A 4-spark annulus ensures centrally-located end gas. The cylinder is imaged from below through a piston crown window, with a 50:50 beamsplitter enabling simultaneous PLIF and flame imaging with an intensified and high-speed camera respectively.

Table 1
Engine specifications.

Bore [mm]	85
Stroke [mm]	90
Fuel injection system	Direct injection
Injection pressure [bar]	200
Inlet valve actuation	Single valve (of two)
Dynamometer	DC, 40 kW

Table 2
Engine instrumentation.

Measured quantity	Sensor
Cylinder pressure	Kistler 6043A60
Barrel pressure	Kistler 4075A10 (with cooling adapter Kistler 7505B)
Inlet pressure	Kistler 4043A5
Manifold pressure	Druck PDCR 820-0800
Exhaust pressure	Kistler 4075A10 (with switching cooling adapter Kistler 7533A)
Air flow rate	Roots meter model 1.5 M125
Inlet temperature	Exposed junction K-type thermocouple
Engine speed	Leine and Linde crank encoder 632006911

to be reached by deflagration would be the central, optically accessible portion. In a typical ignition setup, where charge motion and spark plug placement are optimised for combustion speed and efficiency, the spark is usually centrally mounted, with the flame propagating out from the centre to the cylinder walls—this is incompatible with the objectives of this work. Hence an annulus with four simultaneously triggered spark plugs was designed, in order to produce four flame fronts that travel from the edges of the cylinder inwards. High levels of swirl motion were obtained by disabling the flywheel-side intake valve (Schaeffler UniAir Continuously-Variable Valve Train system) and this setup successfully produced central end gas.

The optical setup to perform PLIF measurements of the central end gas, simultaneously with high-speed imaging of the flame luminosity, is detailed in Fig. 1.

The 3rd harmonic (355 nm) of a 10 Hz, ns-pulse Nd:YAG laser (Continuum Surelite I-10), which had a fluence of 0.05 J/cm^2, was used in combination with sheet forming optics (Thorlabs LK1283L1-A, f = −40 mm cylindrical lens; Thorlabs LA4579-UV-ML, f = 300.0 mm spherical lens) to pass a laser sheet through opposing pentroof windows. This illuminated a horizontal plane within the engine, 3 mm above the firing deck, with approximate dimensions 30 mm × 50 mm × 1 mm, which were determined by using the sheet to illuminate a scale target. The pulse energy at 355 nm was 14 mJ.

A circular piston crown window and a 45-degree mirror within the Bowditch extended piston enabled both formaldehyde fluorescence from the PLIF measurement plane and light emission from the flame to be imaged from below. A 50:50 plate beamsplitter (Thorlabs BSW27) was used to direct light from the engine onto the two detection arms. The beamsplitter's wide range coating (350–1100 nm, as opposed to a typical visible coating range of 400–700 nm) was necessary to avoid ghosting on the flame luminosity images due to partial reflection of light above 800 nm from the rear surface of the beamsplitter.

One detection arm consisted of a high-speed camera (Phantom VEO 710L) using a Nikkor 105 mm lens at f/2.5 to image the flame luminosity at one frame per crank angle. The formaldehyde fluorescence was imaged in the other detection arm using a UV-compatible intensified camera (Andor iStar sCMOS 18U-E4, with a Nikkor 85 mm lens at f/2) which incorporates a WE-AGT photocathode and a fast-decay P46 phosphor (200 ns decay time to 10%), using an intensifier gate time of 1 μs. A bandpass filter (UQG optics CDB-5051) and a longpass filter (UQG optics FGG-39550) were used to transmit the formaldehyde fluorescence with >75% transmission between 400 nm and 470 nm onto the intensified camera, while blocking elastic scatter from the 355 nm excitation sheet with an effective optical density of >10^5.

During the preliminary testing with n-heptane, cylinder head features were visible on the PLIF images, having been illuminated by the fluorescence emission from the measurement plane. Image processing steps in Section 2.3.2 partially mitigated this effect for the n-heptane runs but for all subsequent datasets the cylinder head was painted black to minimise the intensity of these background features.

2.2. Operating conditions

To isolate LTHR, fuel was injected into the motored engine with the ignition system disabled and the inlet air heated, as described by White et al. [38]. Table 3 summarises the operating conditions for the three sets of tests. n-heptane was chosen for the initial motored tests because of its strong LTHR behaviour and hence maximised signal intensity. PRF85 was chosen for the fired tests to maximise LTHR intensity with its n-heptane content but minimise the possibility of engine knock with its relatively high octane rating. The fuels were injected early to give as homogeneous as possible a mixture at the point of LTHR, and previous work has shown that there is a near homogeneous mixture in this engine at this injection timing (albeit at a different operating

Table 3
Engine operating conditions.

Study	Cycle-based	Intra-cycle	Firing
Fuel	n-heptane	PRF85	
Inlet temperature (°C)	60, 100	120	
Ignition timing (°CA aTDC)	N/A		−30, −15
Injection timing (°CA aTDC)	−280		
Engine speed (rpm)	1180		
Equivalence ratio (ϕ)	0, 0.5	0.5	
Inlet pressure (kPa)	80		
Injection pressure (bar)	200		
Air mass flow rate (g/s)	2.75		

point) [42]. With PRF85, the inlet temperature was increased from 100 to 120 °C to account for its lower LTHR propensity. The engine speed was selected to synchronise with the LIF excitation laser's repetition rate of just under 10 Hz (9.83 Hz) — enabling the same crank angle to be imaged cycle-to-cycle. The laser and cameras were triggered from the engine crank at the desired crank angle. To maximise the runtime of the optical engine under fired conditions, the coolant temperature was set to 25 (°C).

The equivalence ratio of $\phi = 0.5$ was chosen to give the best chance of observing LTHR at engine conditions compatible with the optical engine. An equivalence ratio higher than 0.5 would have required increased cylinder pressures and temperatures that exceed the pressure limits of the engine with optical components fitted, but the LTHR behaviour observed in this work at $\phi = 0.5$ would be expected to generalise to higher equivalence ratios, including stoichiometric [35, 41].

As this engine is a direct injection engine, it should be noted that the direct injection causes charge cooling which in turn reduces temperatures and therefore LTHR intensity [41]. At lean equivalence ratios where LTHR was present, ignition was unstable, causing somewhat unreliable combustion that presented itself as alternating firing and misfiring cycles. While nominal fuel and air flow rates were maintained between motored and fired cases, the residuals in the chamber after a failed combustion event made the equivalence ratio of the subsequent cycle slightly richer but ultimately enabled the required sustained combustion within that cycle. Increasing the equivalence ratio in an attempt to reliably fire the engine every cycle was attempted but caused cylinder temperatures to be too low for LTHR to occur due to the additional charge cooling. When analysing the data, fired cycles were filtered and presented.

2.3. Data analysis

2.3.1. Engine data processing

Combustion analysis was performed during post-processing with a MATLAB-based procedure. Cylinder pressure was calibrated with concurrent barrel pressure measurements to avoid drift, and cylinder volume was calculated from the engine geometry. Apparent heat release rate (AHRR) was calculated on a per-cycle basis according to Stone [43]. A median filter was applied to each AHRR cycle before the mean trace was calculated to remove noise. To calculate cumulative heat release (also referred to as LTHR intensity), AHRR for unfuelled, motored, cases were subtracted to account for an approximation for most heat transfer effects.

2.3.2. Image processing

A calibration grid, placed in line with the laser plane, was imaged with all windows installed in the engine and used to transform and spatially calibrate the intensified camera images and high-speed flame images using MATLAB. For the n-heptane tests, the cylinder head was unpainted and strongly illuminated by scattered light and PLIF emission from the laser sheet region, leading to background cylinder head structure being clearly visible in the PLIF frames which could not be removed by subtraction of, for example, the mean image from a non-fuelled run without LTHR due to the PLIF-dependent contribution to the apparent background intensity. To mitigate this, individual PLIF frames (in Fig. 4) were divided by the mean illuminated image to minimise the visibility of the background cylinder head structure and partially correct for spatial variation in laser plane intensity. For the remainder of test points in this work, the cylinder head was painted black and this image correction via division did not need to be applied. Three regions, either could not be painted or were still highly reflective during the tests and were therefore masked out of the images presented in the results; these appear as an annulus around the centrally mounted spark (which was disabled), the area around the pressure transducer and an oval-shaped patch at around (−10, −10).

Regions of formaldehyde were detected in the PLIF images using a MATLAB procedure that applied a median filter, then applied morphological close and open filters to remove speckles and finally applied adaptive thresholding to create a binary image, with the threshold based on the overall brightness of the image. Adaptive thresholding was required due to the nature of scattering—the dark gaps in the plane that did not contain formaldehyde were brighter in bright cycles due to the omnidirectional nature of fluorescence and subsequent scatter. The same method was applied for flame detection without the need for adaptive thresholding. The flame images are presented in this work as flame history images, calculated by taking the maximum pixel intensity for each pixel for the range up to a specified crank angle. This was to ensure that early, bright flame regions that later become dark are taken into account when comparing them to the effects of the flames in the PLIF images.

PLIF signal intensity was calculated by using the above method to identify fluorescing pixels, then summing their intensity and dividing that sum by the number of fluorescing pixels to calculate the mean fluorescing pixel intensity. This was required so that the gaps caused by formaldehyde consumption did not affect indicated LTHR intensity. Shot-to-shot variation in laser intensity and laser sheet spatial inhomogeneity were not corrected for.

For the n-heptane data, the cameras were triggered before the output of the laser had fully stabilised. So, to correct for laser warm-up which manifested as an increase in PLIF intensity over time due to increasing laser pulse energy, a logarithmic curve was fitted to, and subsequently subtracted from, the intensity data. Then, a moving window correlation was calculated by finding the Pearson correlation coefficient, r, between the PLIF and LTHR intensity traces for each pair of cycles and their immediate neighbours.

3. Results and discussion

3.1. Cycle-based PLIF

3.1.1. Qualitative analysis

To qualitatively investigate the effect of LTHR on the PLIF signal, initial tests were carried out with n-heptane, using the isolated LTHR methodology [38] at two inlet temperatures—one where minimal LTHR would be expected and one where relatively high LTHR intensity is common. The apparent heat release rate traces are presented in Fig. 2 and mean PLIF signal images are presented in Fig. 3; baseline traces and images for cases with the injection turned off (i.e. unfuelled motored cases) are also presented, to help distinguish any non-LTHR related signal strength. Examining the baseline AHRR traces reveals them to be effectively identical. Since no fuel is present in these cases, the net heat release — which is negative — can be attributed solely to the effects of heat transfer from the compression-heated air to the walls at lower temperatures. The $T_{in} = 60$ °C case where fuel was injected still shows net negative heat release, though it is up to 0.25 J/°CA more positive than the unfuelled cases, suggesting that LTHR is likely to be occurring, but with very low intensity. Finally, the fuelled $T_{in} = 100$ °C case shows the clear isolated LTHR that has been observed in previous

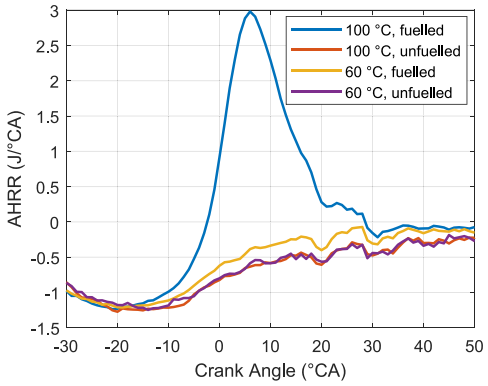

Fig. 2. Apparent heat release rate data for a fuelled and unfuelled engine, motored operation with n-heptane at two inlet temperatures.

studies [38]—with peak AHRR reaching 3 J/°CA.

The four PLIF images presented in Fig. 3 are mean averages of images from over 200 consecutive cycles for each test point; each individual image was taken at 20 °CA aTDC. Formaldehyde is known to be formed during LTHR [9], and under motored conditions, there is no cause for it to be consumed so formaldehyde accumulates in the cylinder until it exits through the exhaust valves. Hence, images captured at 20 °CA aTDC would be expected to show fluorescence from formaldehyde that has accumulated over the course of the cycle. The first thing to note is that the images for the unfuelled cases (i.e. "Injection Off") are not entirely dark — even where no laser sheet structure is present, the shape of the cylinder head can be distinguished. This non-zero PLIF signal may be attributed to background light of a similar wavelength (blue visible) to formaldehyde fluorescence, or to small amounts of fluorescence and subsequent scatter from contaminants such as gasket sealing compound within the pent roof window recesses.

Examining the mean image for the T_{in} = 60 °C case where fuel was injected reveals a slightly brighter signal, most evident in the enhanced visibility of the cylinder head structure; however, the structure of the laser sheet is still not present. The small increase in brightness relative to the unfuelled cases is consistent with Fig. 2 — there is likely very weak LTHR intensity that leads to the formation of relatively small, but non-zero, concentrations of formaldehyde at 20 °CA aTDC. The direct fluorescence is too weak to distinguish but has the effect of raising the overall brightness of the image. Finally, the image for the fuelled T_{in} = 100 °C case is significantly brighter than all other cases. Furthermore, the outline (and to some extent, the structure) of the laser sheet is apparent. This is consistent with the high LTHR intensity AHRR in Fig. 2. Due to scatter, and the fact that the cylinder head surface had not been painted black during these preliminary tests, the brightness in the raw PLIF images does not exclusively correlate with spatial formaldehyde concentration. Hence a strong overall illumination effect is observed for the whole cylinder. Nevertheless, the pair of figures serve as evidence that formaldehyde PLIF can be used to detect the presence of LTHR over averaged cycles—i.e. signal brightness is qualitatively correlated with LTHR.

3.1.2. Individual snapshots

16 individual example frames from the set of images that were used to make the T_{in} = 100 °C image in Fig. 3 are presented in Fig. 4. As described in Section 2.3.2, each snapshot image has been divided by the mean image to partially correct for both laser plane intensity and the contribution from the cylinder head structure. The spatially calibrated frames have been masked to isolate the laser sheet area and are presented in the order in which they were captured. Gas structure is apparent in many of the images, in particular cycle numbers 70, 100, 130 and 190, though some show almost no signs of it, for example, cycle numbers 110, 160 and 200. The cause of the gas-like structures is likely due to inhomogeneities within the temperature and species distributions of the turbulent in-cylinder flow. The hottest regions with the highest local reactivity will experience the most LTHR and produce the most formaldehyde—then, turbulent cylinder flows will transport this formaldehyde around the cylinder and LTHR continues to occur elsewhere. The clarity of these detailed structures within the PLIF images is characteristic of the planar nature of PLIF measurements, as opposed to line-of-sight integrated techniques such as natural light imaging. It is apparent on inspection of the chronologically ordered PLIF images that there is a trend for image brightness to increase over time (cycles). Rather than any gradual increase in LTHR intensity, this can be attributed to laser warm-up for this preliminary dataset. Laser warm-up effects were avoided in the subsequent datasets of Section 3.2 onwards.

3.1.3. Semi-quantitative analysis

Section 3.1.1 demonstrated a qualitative link between LTHR intensity and the brightness of the formaldehyde PLIF signal. The images and thermodynamic data captured at T_{in} = 100 °C can be further analysed to attempt to gain semi-quantitative insights into the relationship between the strength of the PLIF signal and the corresponding LTHR intensity.

The PLIF signal across each image (see Fig. 4) is first spatially averaged, then corrected for gradual laser warm-up by fitting a logarithmic trend to the spatially-averaged brightness vs. cycle number (time) of the set of over 200 PLIF signals for each run. This enables the relative brightness between adjacent cycles to be compared in order to investigate the correlation of PLIF signal intensity with LTHR intensity (note that these tests are isolated LTHR so there is no contribution from deflagration). Fig. 5 shows a representative subset of the min–max normalised cumulative heat release for each cycle, i.e. the LTHR intensity (the blue solid line), alongside the corrected PLIF signal intensity (the black dash-dotted line).

There is an apparent similarity between the two traces—as well as some clear differences. Direct comparison of the two measurements is non-trivial due to the inherent differences in spatial averaging between the whole-cylinder pressure-based technique and single-plane optical technique. However, it is reasonable to expect cycles with more LTHR to have a higher likelihood of having high concentrations of formaldehyde within the PLIF measurement plane, leading to brighter PLIF signals.

This potential relationship is assessed with a rolling correlation coefficient using a window size of three. This describes the local similarity in trends of LTHR and PLIF signal intensities for adjacent cycles (one cycle ahead and one behind). The background of Fig. 5 is coloured according to the calculated correlation coefficient for each cycle, highlighting the strong similarity between LTHR intensity and PLIF signal intensity for the majority of this data subset; as well as notable differences around cycles 39, 48 and 52.

The rolling correlation coefficients for all cycles are summarised in Fig. 6. Over 37% of the total are 0.9 or above and 77% are positive, suggesting that there is a positively correlated relationship between LTHR intensity and PLIF signal from formaldehyde within the measurement plane on a cycle-by-cycle basis.

This is particularly compelling, considering that the PLIF measurement plane represents a very small portion of the cylinder volume (2% at 20 °CA aTDC), the formaldehyde distribution is not homogeneous (as seen in gas structure frames in Fig. 4), and PLIF signal intensity is not expected to be linear with LTHR.

3.2. Ensemble-averaged intra-cycle PLIF

The principal aim of this work is to demonstrate the use of PLIF to detect, and track the progress of LTHR for application in conditions where a pressure-derived method of LTHR tracking cannot be applied. Hence it is necessary to determine whether PLIF signal intensity can

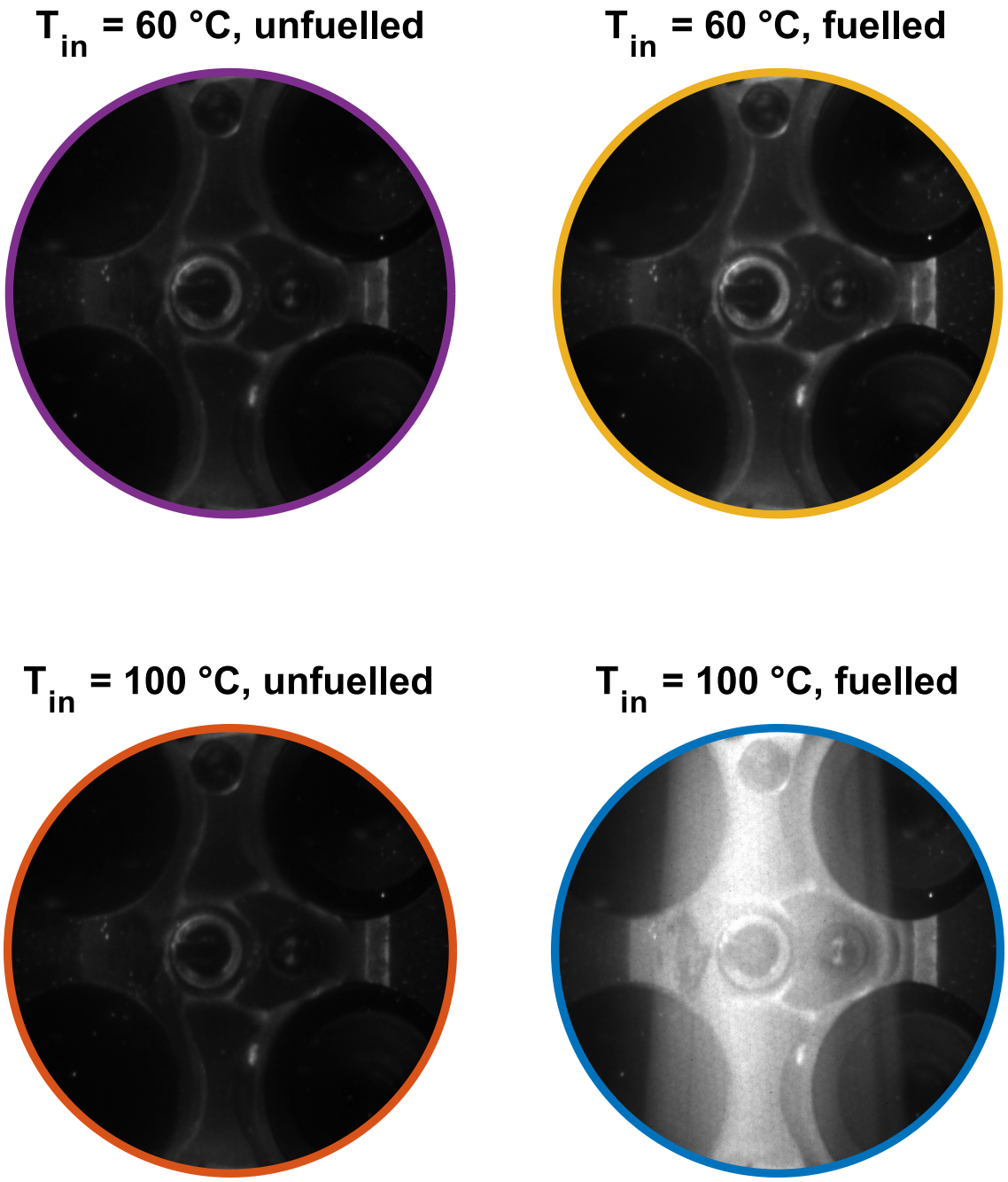

Fig. 3. Average PLIF images captured at 20 °CA aTDC for the four cases in Fig. 2. (For interpretation of the references to colour in this figure legend, the reader is referred to the web version of this article.)

be related to LTHR progress within a cycle. The laser employed was limited to one shot per cycle, so investigations within a single cycle were not possible and ensemble-averaged PLIF and LTHR data were studied instead. A motored test condition producing repeatable pressure-derived LTHR traces (PRF85 at T_{in} = 100 °C) was selected and PLIF images were captured over a wide range of crank angles over sequential cycles.

Formaldehyde formation is used as a marker for LTHR intensity (i.e. the rate of heat release from LTHR) and, in the absence of deflagration, there is no cause for it to be consumed, so for motored cases formaldehyde should accumulate throughout the cycle. Interpretation of the PLIF images as a measure of formaldehyde is complicated by the change in volume as a function of crank angle. This leads to the number density of formaldehyde at each crank angle depending both on the creation and the subsequent compression of formaldehyde created at all preceding crank angles of the cycle. The PLIF signal may also depend on the variation of pressure and temperature as a function of crank angle.

To investigate qualitative relationships, for the range of crank angles near TDC of interest in this work where volume changes are a small (but not negligible) fraction of the total swept volume, corrections for volume, pressure and temperature effects were not attempted.

Fig. 7 shows averaged PLIF images every 5 °CA. The PLIF images show a trend of increasing image brightness with time, despite volume, pressure and temperature trends reversing around TDC. This is especially apparent in the –5 °CA to 10 °CA region where volume, pressure and temperature variation is minimised.

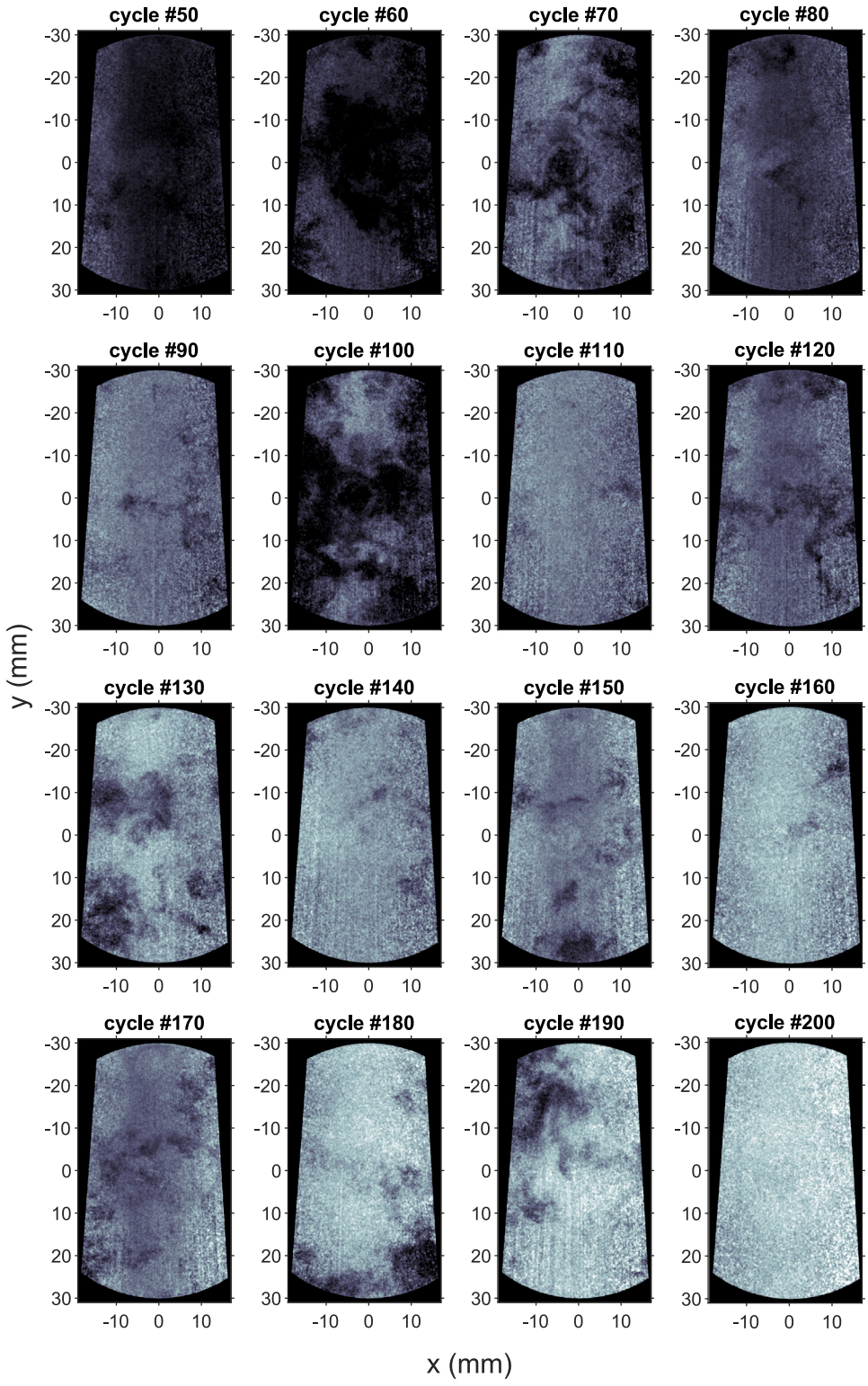

Fig. 4. 16 example PLIF images captured at 20 °CA aTDC, for the engine motored with n-heptane at T_{in} = 100 °C.

Calculating the average cumulative heat release from the pressure traces gives a second accumulating measure of LTHR. If PLIF signal intensity is suitable to use for tracking LTHR processes, there should be a qualitative match between the trends of PLIF signal intensity and cumulative heat release as a function of crank angle for the averaged cycle data.

Min–max normalised traces of average PLIF signal intensity and cumulative heat release are presented in Fig. 8. There is a good level of agreement, considering the cycle-to-cycle variation of the PLIF signal and the uncorrected factors influencing the PLIF signal detailed above, between the two independent methods of following heat release, particularly the timing of their respective greatest rate of change at 0 °CA,

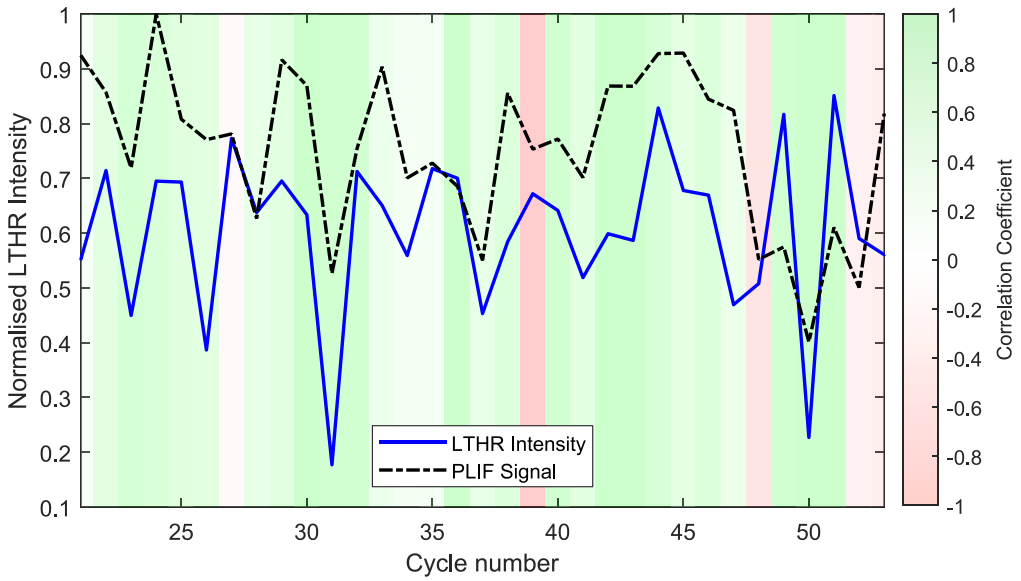

Fig. 5. Cycle-by-cycle LTHR intensity and PLIF signal intensity for a selection of consecutive cycles of motored operation with n-heptane at T_{in} = 100 °C; the similarity in the traces is illustrated with the local correlation coefficient. (For interpretation of the references to colour in this figure legend, the reader is referred to the web version of this article.)

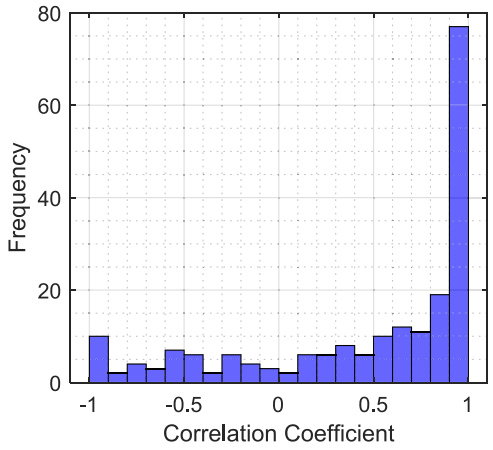

Fig. 6. Distribution of the local correlation coefficients between the LTHR intensity (pressure-based) and the PLIF data for all cycles—engine motored with n-heptane at T_{in} = 100 °C.

supporting the use of formaldehyde PLIF to track LTHR progress within a cycle.

3.3. Simultaneous LTHR and deflagration

As discussed in the introduction, it has recently been theorised that LTHR could be occurring in a volumetric manner in the unburned regions simultaneously alongside deflagration (in contrast to occurring just ahead of the flame as 'cool flame' reactions, which are well-studied). Should this occur, it would not be detectable using standard pressure-based heat release analysis techniques [13]. The deflagration results presented in this work used the four spark ignition setup as described in Section 2.1 as part of the efforts to detect such behaviour. Fig. 9 illustrates this with three apparent heat release rate traces from three different test points: AHRR from an isolated LTHR cycle (Section 3.2) is shown in blue, and AHRR for two firing cases differing only by ignition timing are shown— a later spark timing of −15° aTDC in orange and an earlier spark timing of −30° aTDC in yellow. Note that the AHRR peaks are small in magnitude and long in duration compared to typical work. This is because spark plug placement and cylinder charge motion were not optimised for combustion speed but for optical access of the end gas.

The later ignition case (orange solid line) closely resembles previous PSHR work in the literature [13], with a clear initial heat release peak around 0° aTDC, before the main HTHR from deflagration. Subtracting the AHRR trace of the isolated LTHR case from the later ignition case results in a virtual AHRR trace (orange dashed line) that approximates the HTHR contribution to the later ignition case.

The earlier ignition case (yellow solid line) shows no visible LTHR peak. This is highlighted in Fig. 9 by translating this trace 15 °CA later (yellow dashed line) where it closely resembles the approximated HTHR trace of the later spark timing case. AHRR traces similar to the early spark timing case exhibit no clear signs of LTHR in the pressure trace, so when analysing the formaldehyde PLIF signals for the −30° aTDC ignition case, one might not necessarily expect to see any signals indicating LTHR.

Fig. 10 presents PLIF images from the −30° aTDC spark timing condition and shows that, in fact, there are indications of the occurrence of LTHR in the form of mean PLIF signal intensities which show a notable increase around 0 °CA (top row). These mean PLIF images resemble the isolated LTHR condition of Fig. 7, albeit with reduced intensities at later crank angles.

These reduced mean PLIF intensities are a consequence of the flame intersecting the PLIF measurement plane at later crank angles and consuming the formaldehyde. The middle row of Fig. 10 displays an example single-shot PLIF image for each crank angle and the simultaneous natural light flame history images are presented in the bottom row.

From 10° aTDC onwards, dark regions in the otherwise bright PLIF images qualitatively overlap with the bright flame emission regions in the natural light images. For the example PLIF image at 30° aTDC, the flame has almost completely consumed the formaldehyde within the PLIF measurement plane, leaving only a small bright region to contribute to the mean PLIF image of the top row.

The intensity of these PLIF signals are quantified in Fig. 11, which compares the fired case signal intensity to the motored case from Fig. 8 (the traces are min–max normalised together). To account for the "burnt" regions, the regions of each image where formaldehyde is present were identified and only these regions were used to calculate intensity (as described in Section 2.3.2).

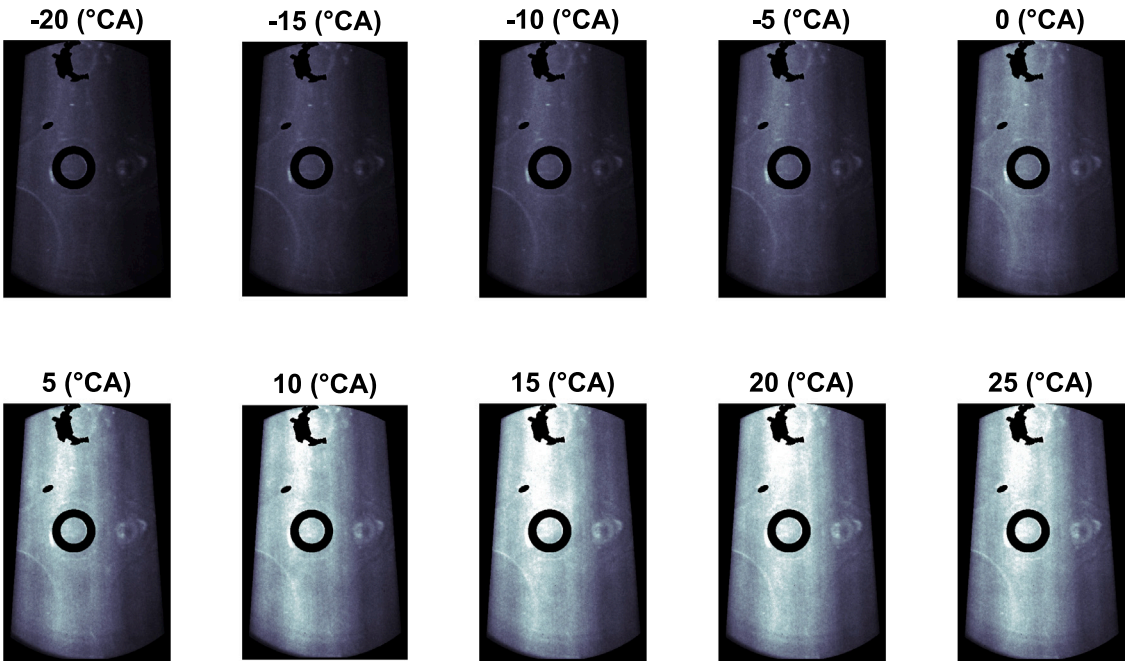

Fig. 7. Average PLIF images captured at 5 °CA increments, for the engine motored with PRF85 at T_{in} = 120 °C in order to induce isolated LTHR.

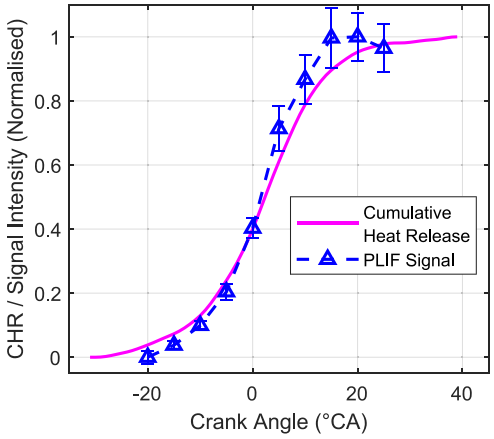

Fig. 8. Min–max normalised cumulative heat release and PLIF signal intensity (of the images in Fig. 7) for an engine motored with PRF85 at T_{in} = 120 °C in order to induce isolated LTHR.

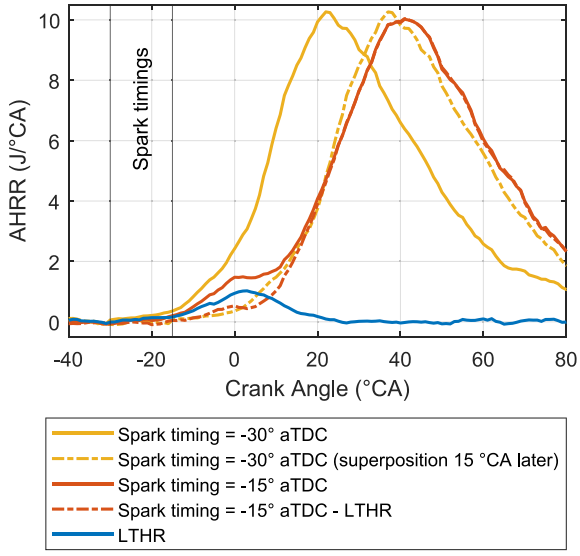

Fig. 9. Apparent heat release rate (AHRR) traces for fired cases at two different spark timings, one with a visible LTHR peak (red) and one without (yellow), compared to a motored case with a visible LTHR peak (blue). (For interpretation of the references to colour in this figure legend, the reader is referred to the web version of this article.)

The two traces exhibit some key similarities and differences. Both cases show a clear sigmoidal shape rise in intensity from −20° aTDC to on or after 20° aTDC, which (as shown in Fig. 8) is consistent with cumulative heat release from LTHR. On the other hand, there is an approximately constant difference in intensity — 0.2 units on the normalised scale — suggesting increased formaldehyde concentration in the motored case compared to the fired case. This can be attributed to a baseline concentration of formaldehyde from residuals present in the motored case, that are not present in the fired case because they are consumed by deflagration. Furthermore, the error bars on the fired case (which correspond to one standard deviation of PLIF signal intensity) are considerably wider for data points at −5° aTDC and later, owing to the cyclic variability caused by combustion—particularly in this setup which was not optimised for combustion speed and stability. The increasing PLIF signal intensity during flame propagation indicates that LTHR is occurring in unburnt regions whilst deflagration contributes to heat release elsewhere in the cylinder. To the best of the authors' knowledge, this is the first time it has been demonstrated in an SI engine. A key implication of these findings is that the chemical composition of the end gas that the flame propagates into will be different to that of the original fuel-air mixture—hence combustion properties such as knocking propensity will be different as a result.

The variations in flame progression inevitably result in cyclic variation in combustion phasing and speed and hence variation in pressure (and temperature) rises. Higher cylinder pressures and certain temperatures (i.e. below the NTC region) are conducive to LTHR. For the PLIF images collected, the cases where deflagration initiated sooner and flames developed earlier often showed large dark patches, but with the remaining signal tending to be brighter due to the elevated pressures and temperatures. This observation is presented semi-quantitatively in Fig. 12, which shows the test cases grouped into three by the start of

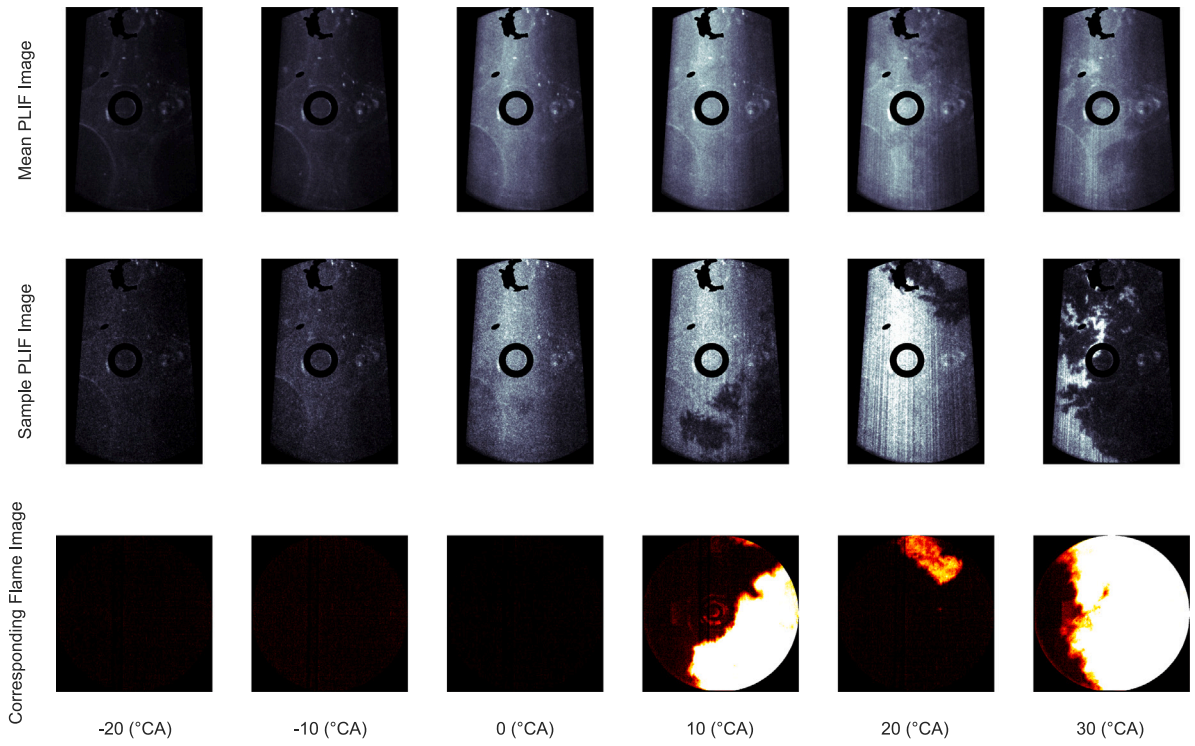

Fig. 10. PLIF and flame history images at a range of crank angles for cycles fired with −30° aTDC spark timing—average PLIF images are presented on the top row, individual sample PLIF frames on the middle row and corresponding flame history images on the bottom row. (For interpretation of the references to colour in this figure legend, the reader is referred to the web version of this article.)

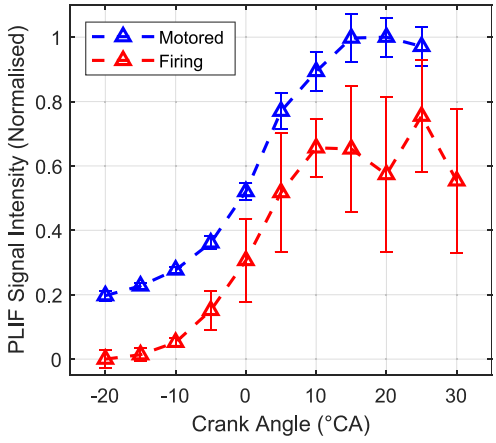

Fig. 11. PLIF Signal intensity for motored, isolated LTHR cycles (blue) and fired cycles (red) with −30° aTDC spark timing. (For interpretation of the references to colour in this figure legend, the reader is referred to the web version of this article.)

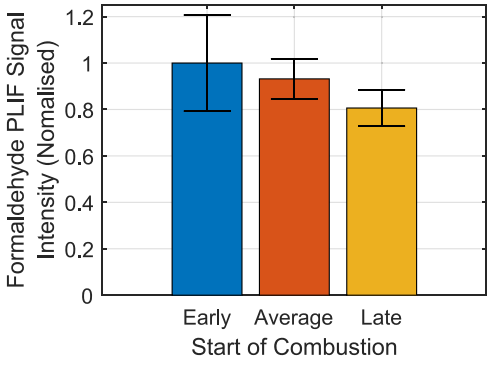

Fig. 12. Effect of combustion phasing (as indexed by start of combustion) on the PLIF signal intensity of the formaldehyde zones in PLIF images from fired cycles with −30° aTDC spark timing.

combustion (defined by the crank angle at which 10% of fuel is burnt) plotted against the intensity of the remaining patches of fluorescence in the PLIF images. It should be clarified that these trends are specific to this engine but indicative of more fundamental behaviour that can be generalised. It was the case that in these tests, the occurrence of the earlier stages of deflagration modified the pressure and therefore temperature of the end gas into conditions that are conducive to LTHR. In other engines, the same phenomena could, for example, increase the temperature too much, such that it enters the NTC region and therefore reduces LTHR intensity.

The link between the dark patches within the formaldehyde PLIF images and the flames was qualitatively demonstrated in Fig. 10 — this relationship was quantified, as demonstrated in Fig. 13.

The left-hand side column depicts four example PLIF frames with the dark patches (the gaps in fluorescence) outlined in orange. As in previous images, portions of the cylinder head paint that failed to reduce scatter (such as around the spark plug and pressure transducer) are masked out and appear black. The right-hand side shows the corresponding flame history images, generated by taking the maximum pixel intensity until the time the PLIF image was captured. This is to ensure early bright regions that become dark by the time the PLIF image is taken are still taken into account. This does assume an overall charge motion that is slow relative to the flame propagation speed. Gas velocities were not measured in this work, but the results of Fig. 14 (discussed later) are consistent with this assumption. Flame history is then detected and outlined in cyan. In the centre column, both the dark zones from the PLIF images (orange) and the flame history zones (cyan) are presented for direct comparison and overlaid on a grayscale image of the flame history.

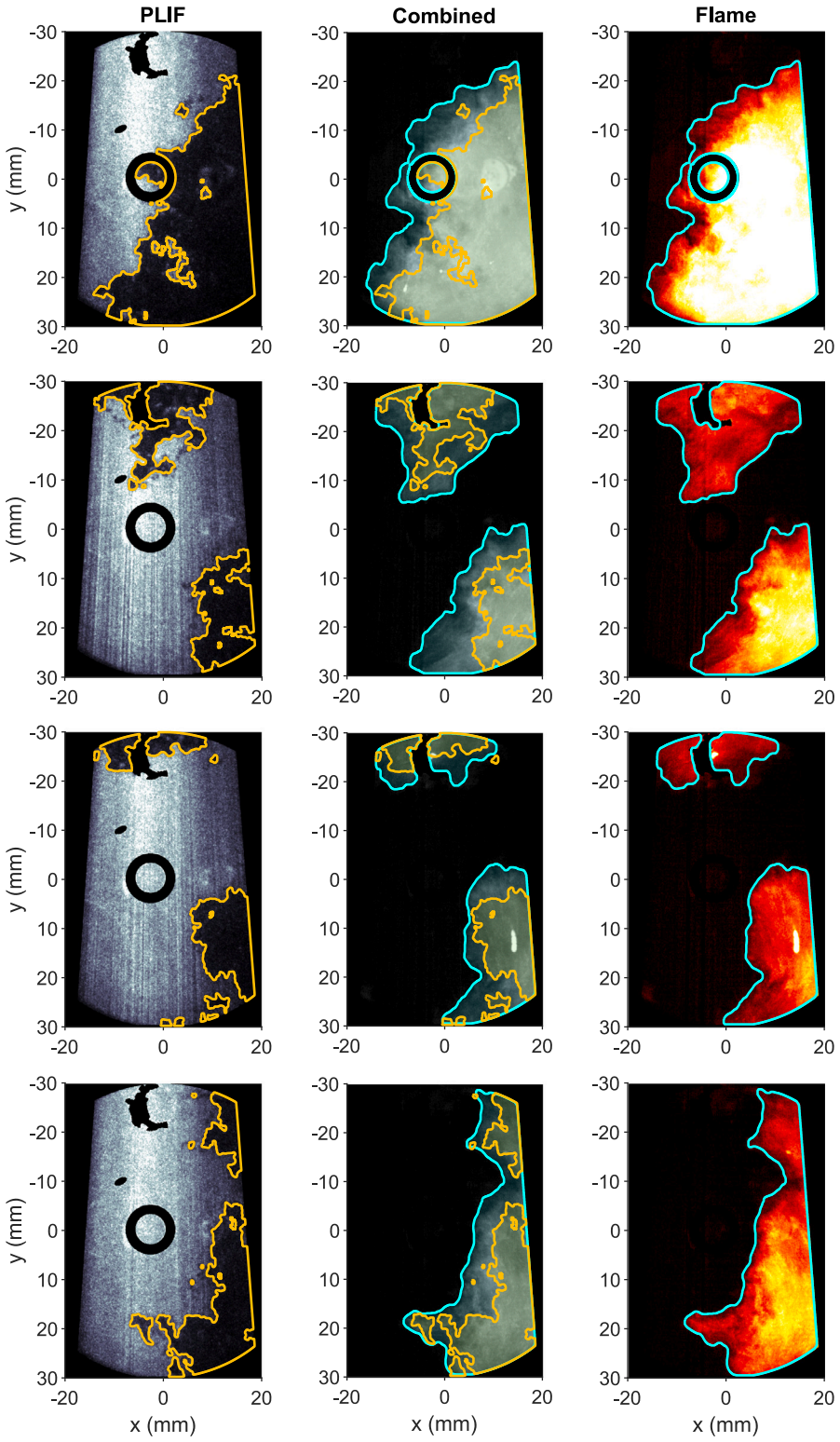

Fig. 13. Spatially calibrated formaldehyde PLIF (left column) and flame history images (right column) captured simultaneously for fired cycles with −30° aTDC spark timing—burnt zones are highlighted and compared in the middle column. (For interpretation of the references to colour in this figure legend, the reader is referred to the web version of this article.)

The independently determined zones show significant similarity — the formaldehyde gaps (highlighted in orange) are almost exclusively located within the flame history zone. This is not entirely surprising as the flame images are line-of-sight integrated whilst the PLIF image samples a relatively thin plane within the cylinder. Any flame activity outside of the laser plane will be detected in the natural light imaging

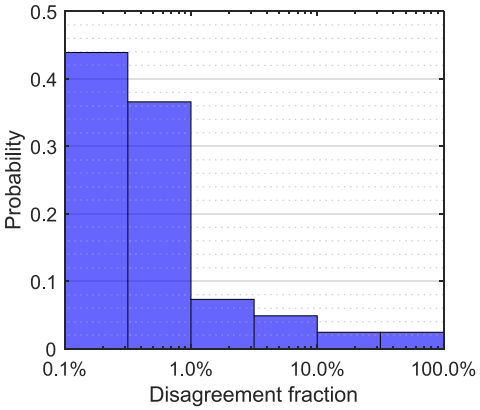

Fig. 14. Distribution of 'Disagreement fraction'—the fraction of the burnt zone in the PLIF images that appear outside of the burnt zone in the flame history images.

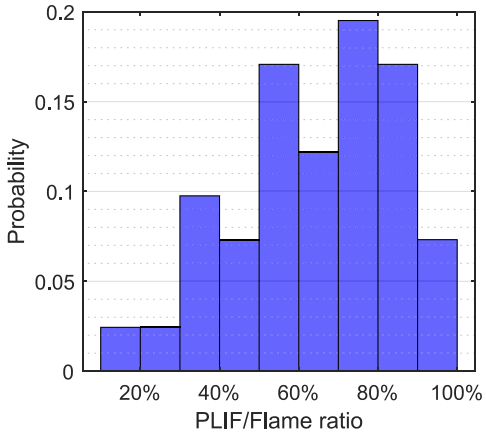

Fig. 15. The ratio of the number of pixels in the burnt zone of the PLIF images to the number of pixels in the burnt zone of the flame history images, plotted as a distribution.

but will not consume the formaldehyde within the plane and hence will not cause a dark patch in the PLIF image. On the other hand, if a dark patch appears in the PLIF image, it will almost certainly have been caused by flame presence and hence that portion of the flame will be detected in the natural light imaging.

Fig. 13's middle column qualitatively shows good agreement between zones from the two independent imaging techniques for the example images presented. The overall similarity between the full set of cycles imaged is quantified in Figs. 14 and 15.

The extent to which the PLIF dark patches (the gaps in fluorescence signal indicating lack of formaldehyde presence) appear outside of the flame zone can be described as the disagreement fraction — the fraction of dark patch pixels that appear outside of the flame zone region. A histogram plot of the disagreement fraction can be seen in Fig. 14. In 80% of cases, the disagreement fraction is 1% or less, suggesting that across the images, the gaps in visible formaldehyde fluorescence can be attributed to formaldehyde consumption by the flame with very high confidence. It is also consistent with the earlier assumption that overall charge motion was slow relative to the flame propagation speed.

The proportion of flame zone occupied by the PLIF dark patches (by number of pixels) is defined as the 'PLIF/Flame' ratio and is presented in Fig. 15. Typically, the dark patches occupied a large proportion of the flame zone, with three-quarters of the image pairs having a ratio of over 50%, and the modal ratio was in the range 70%–80%. Again, this shows good similarity between the methods, considering it would not be expected to be too close to 100% since the PLIF images were planar and flame history images were line-of-sight integrations.

4. Conclusions

In this work, n-heptane and PRF85 were injected into a motored, optically accessible, engine to determine the utility of formaldehyde planar laser-induced fluorescence (PLIF) for observing and tracking low temperature heat release (LTHR) without relying on pressure measurement-based methods. The engine was then fired with four side-mounted spark plugs in order to observe the end gas through the engine's piston window. PLIF was used to track the progression of LTHR occurring in the end gas while high speed natural light flame imaging was used to track the progress of deflagration.

The results show that:

1. For motored conditions, a strong formaldehyde PLIF signal is present when isolated LTHR occurs but not otherwise.
2. Cycle-based PLIF signal intensity within the selected 2D measurement plane is well correlated with total heat released from LTHR on a cyclic basis, despite the relatively small sampling area of the PLIF images.
3. Formaldehyde PLIF signal intensity can be used to track LTHR progression within a cycle due to its strong relationship with cumulative heat release, as evaluated using ensemble-averaged data.
4. Formaldehyde in the end gas, produced by LTHR is consumed by deflagration, which makes the presence of flames visible in PLIF images as dark regions. There was good agreement between formaldehyde PLIF images of firing cycles and natural light flame history images, as measured independently by a high speed camera.
5. The PLIF technique was able to observe LTHR in firing engine cycles where the apparent heat release data exhibited no distinguishable indications of LTHR.

This work has shown simultaneous volumetric low temperature heat release and deflagration in a spark ignition engine for the first time when other methods (i.e. pressure-derived heat release analysis) are unable to observe LTHR. The occurrence of this end gas LTHR has important implications for combustion behaviour, namely that the chemical composition of the end gas that the flame propagates into will be different to that of the original fuel-air mixture, hence combustion characteristics such as knocking propensity will differ.

Nomenclature

°CA	Crank angle degrees
HCCI	Homogeneous charge compression ignition
LTHR	Low temperature heat release
NTC	Negative temperature coefficient
P	Pressure
PLIF	Planar laser-induced fluorescence
PSHR	Pre-spark heat release
SI	Spark ignition
SICI	Spark induced compression ignition
T	Temperature
TDC	Top dead centre
ϕ	Fuel-air equivalence ratio

CRediT authorship contribution statement

Samuel P. White: Writing – original draft, Visualization, Methodology, Investigation, Formal analysis, Conceptualization. **Christopher Willman:** Writing – original draft, Methodology, Investigation, Data curation. **Felix C.P. Leach:** Writing – review & editing, Supervision, Project administration, Funding acquisition, Conceptualization.

Declaration of competing interest

The authors declare that they have no known competing financial interests or personal relationships that could have appeared to influence the work reported in this paper.

Acknowledgements

This research was supported by an Engineering and Physical Sciences Research Council Prosperity Partnership, UK, grant number EP/T005327/1. For the purpose of Open Access, the authors have applied a CC BY public copyright license to any Author Accepted Manuscript (AAM) version arising from this submission. The Prosperity Partnership is a collaboration between JLR, Siemens Digital Industries Software, the University of Bath, and the University of Oxford. The authors would also like to thank Dr Priyav Shah and Professor Ben Williams for experimental setup support and the Dept. of Engineering Science technicians and maintenance teams for facilities support.

Data availability

The data that has been used is confidential.

References

[1] Leach F, Kalghatgi G, Stone R, Miles P. The scope for improving the efficiency and environmental impact of internal combustion engines. Transp Eng 2020;1:100005. http://dx.doi.org/10.1016/j.treng.2020.100005.

[2] Wang Z, Liu H, Reitz RD. Knocking combustion in spark-ignition engines. Prog Energ Combust 2017;61:78–112. http://dx.doi.org/10.1016/j.pecs.2017.03.004.

[3] Livengood J, Wu P. Correlation of autoignition phenomena in internal combustion engines and rapid compression machines. Symp (Int) Combust 1955;5(1):347–56. http://dx.doi.org/10.1016/S0082-0784(55)80047-1.

[4] Leppard WR. The chemical origin of fuel octane sensitivity. SAE Tech. Pap. 902137, 1990, http://dx.doi.org/10.4271/902137.

[5] Shibata G, Oyama K, Urushihara T, Nakano T. The effect of fuel properties on low and high temperature heat release and resulting performance of an HCCI engine. SAE Tech. Pap. 2004-01-0553, 2004, http://dx.doi.org/10.4271/2004-01-0553.

[6] Shibata G, Oyama K, Urushihara T, Nakano T. Correlation of low temperature heat release with fuel composition and HCCI engine combustion. SAE Tech. Pap. 2005-01-0138, 2005, http://dx.doi.org/10.4271/2005-01-0138.

[7] Truedsson I, Cannella W, Johansson B, Tuner M. Engine speed effect on autoignition temperature and low temperature reactions in HCCI combustion for primary reference fuels. SAE Tech. Pap. 2014-01-2666, 2014, http://dx.doi.org/10.4271/2014-01-2666.

[8] Curran HJ, Gaffuri P, Pitz WJ, Westbrook CK. A comprehensive modeling study of iso-octane oxidation. Combust Flame 2002;129(3):253–80. http://dx.doi.org/10.1016/S0010-2180(01)00373-X.

[9] Curran H, Gaffuri P, Pitz W, Westbrook C. A comprehensive modeling study of n-heptane oxidation. Combust Flame 1998;114(1):149–77. http://dx.doi.org/10.1016/S0010-2180(97)00282-4.

[10] Szybist JP, Splitter DA. Pressure and temperature effects on fuels with varying octane sensitivity at high load in SI engines. Combust Flame 2017;177:49–66. http://dx.doi.org/10.1016/j.combustflame.2016.12.002.

[11] Splitter D, Kaul B, Szybist J, Jatana G. Engine operating conditions and fuel properties on pre-spark heat release and SPI promotion in SI engines. SAE Int J Engines 2017;10(3):1036–50. http://dx.doi.org/10.4271/2017-01-0688.

[12] Waqas MU, Hoth A, Kolodziej CP, Rockstroh T, Gonzalez JP, Johansson B. Detection of low temperature heat release (LTHR) in the standard cooperative fuel research (CFR) engine in both SI and HCCI combustion modes. Fuel 2019;256:115745. http://dx.doi.org/10.1016/j.fuel.2019.115745.

[13] Splitter DA, Gilliam A, Szybist J, Ghandhi J. Effects of pre-spark heat release on engine knock limit. P. Combust Inst 2019;37(4):4893–900. http://dx.doi.org/10.1016/j.proci.2018.05.145.

[14] Urushihara T, Yamaguchi K, Yoshizawa K, Itoh T. A study of a gasoline-fueled compression ignition engine ∼ expansion of HCCI operation range using SI Combustion as a trigger of compression ignition ∼. SAE Tech. Pap. 2005-01-0180, 2005, http://dx.doi.org/10.4271/2005-01-0180.

[15] Ma X, Wang Z, Jiang C, Jiang Y, Xu H, Wang J. An optical study of in-cylinder CH_2o and OH chemiluminescence in flame-induced reaction front propagation using high speed imaging. Fuel 2014;134:603–10. http://dx.doi.org/10.1016/j.fuel.2014.06.002.

[16] Hu Z, Zhang J, Sjöberg M, Zeng W. The use of partial fuel stratification to enable stable ultra-lean deflagration-based spark-ignition engine operation with controlled end-gas autoignition of gasoline and E85. Int J Engine Res 2020;21(9):1678–95. http://dx.doi.org/10.1177/1468087419889702.

[17] Bajwa AU, Leach FCP, Davy MH. Prospects of controlled auto-ignition based thermal propulsion units for modern gasoline vehicles. Energ 2023;16(9):3887. http://dx.doi.org/10.3390/en16093887.

[18] Martz J, Kwak H, Im H, Lavoie G, Assanis D. Combustion regime of a reacting front propagating into an auto-igniting mixture. P. Combust Inst 2011;33(2):3001–6. http://dx.doi.org/10.1016/j.proci.2010.07.040.

[19] Suzuki R, Shoji H, Yoshida K, Iijima A. Analysis of knocking in an SI engine based on in-cylinder: spectroscopic measurements and visualization. SAE Tech. Pap 2010-32-0092, 2010, http://dx.doi.org/10.4271/2010-32-0092.

[20] Eckbreth A. Laser diagnostics for combustion temperature and species. 2nd ed.. Gordon and Breach Publishers; 1996, http://dx.doi.org/10.1201/9781003077251.

[21] Zhao H, Ladommatos N. Engine combustion instrumentation and diagnostics. SAE International; 2001, URL: http://books.sae.org/r-264/.

[22] Jeffries JB, Kohse-Höinghaus K. Applied combustion diagnostics. 1st ed.. London: Taylor & Francis; 2002.

[23] Schulz C, Dreizler A, Ebert V, Wolfrum J. Combustion diagnostics. In: Tropea C, Yarin AL, Foss JF, editors. Springer handbook of experimental fluid mechanics. Springer Berlin Heidelberg; 2007, p. 1241–315. http://dx.doi.org/10.1007/978-3-540-30299-5_20.

[24] Schulz C, Sick V. Tracer-LIF diagnostics: quantitative measurement of fuel concentration, temperature and fuel/air ratio in practical combustion systems. Prog Energ Combust 2005;31(1):75–121. http://dx.doi.org/10.1016/j.pecs.2004.08.002.

[25] Sjoholm J, Rosell J, Li B, Richter M, Li Z, Bai XS, Alden M. Simultaneous visualization of OH, CH, CH_2O and toluene PLIF in a methane jet flame with varying degrees of turbulence. P. Combust Inst 2013;34(1):1475–82. http://dx.doi.org/10.1016/j.proci.2012.05.037.

[26] Carter CD, Skiba AW, Boxx I, Allison PM. Optimal approaches to formaldehyde planar laser-induced fluorescence. Combust Flame 2022;246:112431. http://dx.doi.org/10.1016/j.combustflame.2022.112431.

[27] Brackmann C, Nygren J, Bai X, Li Z, Bladh H, Axelsson B, Denbratt I, Koopmans L, Bengtsson PE, Aldén M. Laser-induced fluorescence of formaldehyde in combustion using third harmonic Nd:YAG laser excitation. Spectrochim Acta A 2003;59(14):3347–56. http://dx.doi.org/10.1016/S1386-1425(03)00163-X.

[28] Donkerbroek AJ, van Vliet AP, Somers LM, Frijters PJ, Klein-Douwel RJ, Dam NJ, Meerts WL, ter Meulen JJ. Time- and space-resolved quantitative LIF measurements of formaldehyde in a heavy-duty diesel engine. Combust Flame 2010;157(1):155–66. http://dx.doi.org/10.1016/j.combustflame.2009.07.004.

[29] Thering H, Beckmann L, Jördens C, Röder M, Dreier T, Schulz C. Formaldehyde laser-induced fluorescence imaging with a multi-band transmission filter. Opt Lett 2014;39(7):1873. http://dx.doi.org/10.1364/OL.39.001873.

[30] Schießl R, Maas U. Analysis of endgas temperature fluctuations in an SI engine by laser-induced fluorescence. Combust Flame 2003;133(1–2):19–27. http://dx.doi.org/10.1016/S0010-2180(02)00538-2.

[31] Bäuerle B, Hoffmann F, Behrendt F, Warnatz J. Detection of hot spots in the end gas of an internal combustion engine using two-dimensional LIF of formaldehyde. Symp (Int) Combust 1994;25(1):135–41. http://dx.doi.org/10.1016/S0082-0784(06)80637-5.

[32] Dubreuil A, Mounaïm-Rousselle C, Foucher F, Dagaut P. Comparison between LIF measurements and modeling predictions of OH-HCHO during HCCI mode combustion development. SAE Tech. Pap. 2007-24-0019, 2007, http://dx.doi.org/10.4271/2007-24-0019.

[33] Collin R, Nygren J, Richter M, Aldén M, Hildingsson L, Johansson B. Simultaneous OH- and formaldehyde-LIF measurements in an HCCI engine. SAE Tech. Pap. 2003-01-3218, 2003, http://dx.doi.org/10.4271/2003-01-3218.

[34] Olofsson J, Seyfried H, Richter M, Aldén M, Vressner A, Hultqvist A, Johansson B, Lombaert K. High-speed LIF imaging for cycle-resolved formaldehyde visualization in HCCI combustion. SAE Tech. Pap. 2005-01-0641, 2005, http://dx.doi.org/10.4271/2005-01-0641.

[35] Splitter DA, Gilliam A, Szybist J, Ghandhi J. Effects of pre-spark heat release on engine knock limit. P. Combust Inst 2019;37(4):4893–900. http://dx.doi.org/10.1016/j.proci.2018.05.145.

[36] Graf N, Gronki J, Schulz C, Baritaud T, Cherel J, Duret P, Lavy J. In-cylinder combustion visualization in an auto-igniting gasoline engine using fuel tracer- and formaldehyde-LIF imaging. In: International spring fuels & lubricants meeting. SAE International; 2001, http://dx.doi.org/10.4271/2001-01-1924.

[37] Strozzi C, Claverie A, Prevost V, Sotton J, Bellenoue M. HCCI and SICI combustion modes analysis with simultaneous PLIF imaging of formaldehyde and high-speed chemiluminescence in a rapid compression machine. Combust Flame 2019;202:58–77. http://dx.doi.org/10.1016/j.combustflame.2019.01.002.

[38] White SP, Bajwa AU, Leach FCP. Isolated low temperature heat release in spark ignition engines. SAE Int J Adv Curr Pr Mobil 2024;6(2):827–40. http://dx.doi.org/10.4271/2023-01-0235.

[39] White SP, Bajwa AU, Leach FCP. Effect of ethanol and iso-octane blends on isolated low temperature heat release in a spark ignition engine. SAE Int J Fuels Lubr 2024;17(3). http://dx.doi.org/10.4271/04-17-03-0016.

[40] White SP, Bajwa AU, Leach FCP. Effects of nitric oxide on isolated low temperature heat release in spark ignition engines. Combust Flame 2025. http://dx.doi.org/10.1016/j.combustflame.2024.113921.

[41] Bajwa AU, White SP, Leach FCP. Low temperature heat release and phi-sensitivity characteristics of iso-octane/air mixtures. Combust Sci Technol 2025;197:440–62. http://dx.doi.org/10.1080/00102202.2023.2245635.

[42] Williams B, Ewart P, Wang X, Stone R, Ma H, Walmsley H, Cracknell R, Stevens R, Richardson D, Fu H, Wallace S. Quantitative planar laser-induced fluorescence imaging of multi-component fuel/air mixing in a firing gasoline-direct-injection engine: Effects of residual exhaust gas on quantitative PLIF. Combust Flame 2010;157(10):1866–78. http://dx.doi.org/10.1016/j.combustflame.2010.06.004.

[43] Stone CR. Introduction to internal combustion engines, 4th ed.. Macmillan International Higher Education; 2012.